Correlations in microscopic optical model for nucleon elastic scattering off doubly closed-shell nuclei

M. Dupuis, S. Karataglidis,* E. Bauge, J. P. Delaroche, and D. Gogny†
Commissariat à l'Energie Atomique, Département de Physique Théorique et Appliquée, Service de Physique Nucléaire, Boite Postale 12, F-91680 Bruyères-le-Châtel, France
(Received 17 March 2005; published 23 January 2006)

The random phase approximation (RPA) long-range correlations are known to play a significant role in understanding the depletion of single particle-hole states observed in (e, e') and $(e, e'p)$ measurements. Here the RPA theory, implemented using the D1S force is considered for the specific purpose of building correlated ground states and related one-body density matrix elements. These may be implemented and tested in a fully microscopic optical model for NA scattering off doubly closed-shell nuclei. A method is presented to correct for the correlations overcounting inherent to the RPA formalism. One-body density matrix elements in the uncorrelated (i.e., Hartree-Fock) and correlated (i.e., RPA) ground states are then challenged in proton scattering studies based on the Melbourne microscopic optical model to highlight the role played by the RPA correlations. Agreement between the parameter free scattering predictions and measurements is good for incident proton energies ranging from 200 MeV down to approximately 60 MeV and becomes gradually worse in the lower energy range. Those features point unambiguously to the relevance of the g-matrix method to build microscopic optical model potentials at medium energies, and emphasize the need to include nucleon-phonon coupling, that is, a second-order component of the Feshbach type in the potential at lower energies. Illustrations are given for proton scattering observables measured up to 201 MeV for the ^{16}O, ^{40}Ca, ^{48}Ca, and ^{208}Pb target nuclei.

DOI: 10.1103/PhysRevC.73.014605 PACS number(s): 21.10.Gv, 24.10.Ht, 25.40.Cm, 25.40.Dn

I. INTRODUCTION

Our understanding of the many facets of the nuclear structure properties has been and still is reliant on the picture of independent particles moving in a mean potential. This picture stands at the foundation of the shell model that nowadays serves routinely as the basis of nuclear structure calculations and is implicit to the self-consistent mean-field (i.e., Hartree-Fock) description of nuclear ground states. For independent particle motion, the occupancy associated to nucleon orbitals is 1 or 0 depending on whether the single-particle level is below or above the Fermi energy, respectively.

It is only recently that the quenching of shell-model occupation probabilities has been disclosed in a dedicated series of experiments in which incident electrons serve to map detailed structure properties hard to reach using other probes. First hints revealing such a quenching came in measurements of electron scattering from ^{206}Pb and ^{205}Tl, from which the $3s_{1/2}$ proton radial wave function was determined. Its shape is peaked in the central region and close to expectations for a $3s_{1/2}$ wave function. Minor adjustment of the $3s$-hole strength provided an improved data prediction [1]. Evidence for partial occupancy for this orbital was provided later on from a joint analysis of (e, e'') and $(e, e'p)$ experiments. The $3s_{1/2}$ orbital was found to be depleted by a $(18 \pm 9)\%$ amount [2,3]. Today the absolute occupation probability of this proton orbital is evaluated to be 0.76 ± 0.07 [4].

Further detailed information on the single-particle structure have been recently gained through measurements of the spectral function $S(E, k)$, where E and k are the removal energy and momentum, respectively, of a proton in $(e, e'p)$ knockout experiments. For ^{208}Pb, these measurements performed at high binding energy and momentum transfer show that mean-field predictions are lying far below the data, highlighting the need for consideration of tensor [5,6] as well as short- [7–9] and long-range correlations beyond the mean field [10–13]. A wealth of methods and models have been adopted to tackle this issue. These are the Green's functions method [14,15], the variational Monte Carlo method [16,17], the correlated basis function theory [18], the particle-vibration model [19], the dispersive optical model extrapolated to the bound-state region [20–23], and the random phase approximation (RPA) [24–28]. Among the correlations that have been considered so far, the long-range ones appear important for curing the deficiencies associated with the mean-field predictions.

In the present work we investigate the impact that nuclear long-range correlations have on the interaction of nucleons incident on doubly closed-shell nuclei, among which includes ^{208}Pb, a nucleus for which many scattering observables have been measured. In the past, detailed experimental information on nuclear structure as gained from electron scattering measurements played a key role in building effective NN forces and mass operators for nucleon scattering studies in the folding model framework [29,30]. Now that a successful and parameter free NA microscopic optical model (OM) based on a g-matrix interaction has been established in r space [31],

*Present address: School of Physics, University of Melbourne, Victoria 3010, Australia.
†Present address: Lawrence Livermore National Laboratory, California, USA.

it is timely to push the limits of its predictive power using various microscopic structure information. Several studies along this line have already been published. For example, no core shell-model wave functions have been adopted in successful interpretations of proton scattering measurements for ^{12}C and light nuclei below and at the neutron drip line [32–34]. Hartree-Fock predictions based on Skyrme forces have also been challenged in proton and neutron elastic scattering studies at medium energy to provide estimates of neutron skin thickness in ^{208}Pb. Here, the correlated ground states of stable doubly closed-shell nuclei, built using the finite range, density-dependent D1S force [35] in the self-consistent RPA theory [36], are used instead and thoroughly tested.

Our article is organized as follow. The main features of the fully antisymmetric, microscopic NA optical model are described in Sec. II. Section III includes a brief presentation of the HF+RPA theory for establishing our notations and describes the method used to fix the well-known double counting problem. RPA predictions are compared to experimental data for charge and neutron radial shapes of ^{208}Pb in its ground state. One-body density matrix elements in the correlated ground state are then provided. Finally, optical model predictions based on HF and HF+RPA one-body density matrix elements are compared in Sec. IV to various scattering observables in the 40–201 MeV incident proton energy range for ^{16}O, ^{40}Ca, ^{48}Ca, and ^{208}Pb and to scattering predictions based on the Skyrme SkM* [37] force. These predictions are of good quality only for the higher incident energies. The origin of poorer predictions at the lower energies is discussed in terms of second-order components of Feshbach type, which are missing in the present optical model potential.

II. MICROSCOPIC OPTICAL POTENTIAL FROM THE MELBOURNE *g* MATRIX

The full details of the Melbourne g matrix optical potential may be found in Ref. [31], to which we refer the reader. We present a brief summary of the derivation of the potential, highlighting those points relevant to the use of RPA densities in its calculation and the observables obtained therefrom.

In folding models of the optical potential, one starts with a credible effective *NN* interaction. In the case of the Melbourne potential, the effective *NN* interaction is the g matrix derived from the Bonn-B *NN* interaction [38]. The g matrix for infinite matter is a solution of the Bruckner-Bethe-Goldstone equation in momentum space, *viz.*

$$g(\mathbf{q}', \mathbf{q}; \mathbf{K}) = V(\mathbf{q}', \mathbf{q}) + \int V(\mathbf{q}', \mathbf{k}') \times \frac{Q(\mathbf{k}', \mathbf{K}; k_f)}{[E(\mathbf{k}, \mathbf{K}) - E(\mathbf{k}', \mathbf{K})]} g(\mathbf{k}', \mathbf{q}; \mathbf{K})\, d\mathbf{k}', \quad (1)$$

where $Q(\mathbf{k}', \mathbf{K}; k_f)$ is a Pauli operator and medium effects are included in the energy denominator. Effective g matrices are obtained in coordinate space for finite nuclei whose Fourier transforms best map those momentum space solutions. Those g matrices so obtained contain central, tensor, and two-body spin-orbit terms. They are also constructed over all two-body spin and isospin channels, allowing for a self-consistent specification of proton and neutron scattering, as well as charge exchange reactions. Those g matrices are then folded with the ground-state density matrix elements to give the optical potential for elastic scattering.

The optical potential (OMP) derived therefrom can be cast in the following form:

$$\begin{aligned} U(\mathbf{r}, \mathbf{r}'; E) &= \delta(\mathbf{r} - \mathbf{r}') \sum_{\alpha\beta} \rho_{\alpha\beta} \int \varphi^*_\alpha(\mathbf{s}) g_D(\mathbf{r}, \mathbf{s}; E) \varphi_\beta(\mathbf{s})\, d\mathbf{s} \\ &\quad + \sum_{\alpha\beta} \rho_{\alpha\beta} \varphi^*_\alpha(\mathbf{r}) g_E(\mathbf{r}, \mathbf{r}'; E) \varphi_\beta(\mathbf{r}') \\ &= U_D(\mathbf{r}; E)\delta(\mathbf{r} - \mathbf{r}') + U_E(\mathbf{r}, \mathbf{r}'; E), \end{aligned} \quad (2)$$

where the subscripts D and E designate the direct and exchange contributions, respectively. The density matrix element $\rho_{\alpha\beta}$ is defined in terms of the RPA (or HF) ground state $|0\rangle$ by $\rho_{\alpha\beta} = \langle 0|a^+_\alpha a_\beta|0\rangle$ (see Sec. III). Nuclear structure information enters the construction of the optical potential in two ways. The first one is via the density dependence of the g matrix at the two radii $\mathbf{r}$ and $\mathbf{r}'$. The second one is via the one-body matrix elements $\rho_{\alpha\beta}$ and the specification of the bound-state single-particle wave functions φ_α and φ_β. Note that in Eq. (2), the local and nonlocal radial densities associated to the target ground state can be recognized, namely

$$\begin{aligned} \rho(\mathbf{r}) &= \sum_{\alpha\beta} \rho_{\alpha\beta} \varphi^*_\alpha(\mathbf{r}) \varphi_\beta(\mathbf{r}) \quad \text{and} \\ \rho(\mathbf{r}, \mathbf{r}') &= \sum_{\alpha\beta} \rho_{\alpha\beta} \varphi^*_\alpha(\mathbf{r}) \varphi_\beta(\mathbf{r}'), \end{aligned} \quad (3)$$

respectively. These features clearly show that this kind of potential cannot be constructed from phenomenological nuclear densities. Indeed experimental local densities can be obtained for neutron and charge local radial distributions, but experimental information on nonlocal densities is not available.

The main source of nonlocality in the optical potential is from the exchange term. The direct term resembles a $g\rho$-type optical potential and by definition is local. The form of the exchange term necessarily does not follow this construction: the exchange terms in the folding require that the sum is over explicit effective *NN* two-body amplitudes. As such, direct comparisons are not possible between this form of the optical potential and those that are local, as constructed from nonlocal *NN* amplitudes through local approximations, or as specified phenomenologically as sums of Woods-Saxon form factors.

To obtain the observables for scattering, the optical potential so obtained is used in the nonlocal integrodifferential Schrödinger equation, *viz.*

$$\left[\frac{\hbar^2}{2\mu}\nabla^2 - V_C(r) + E\right]\Psi(\mathbf{r}) = \int U(\mathbf{r}, \mathbf{r}')\Psi(\mathbf{r}')d\mathbf{r}', \quad (4)$$

where $V_C(r)$ is the Coulomb potential and the terms because of the intrinsic spin of the system have been suppressed for simplicity. The code DWBA98 [39] is used to calculate the folding potential from the effective *NN* g matrices and obtain the relevant scattering observables.

At low energy, the averaging over the coupling to the nonelastic channels represented by the g matrix is no longer valid and the derivation of the optical potential must be done in terms of explicit channel coupling to open and closed channels. Such has recently been constructed in terms of the collective model [40,41].

III. NUCLEAR STRUCTURE

As an introduction to this section, it is important to mention that our approach is not fully consistent. On the one hand, we use the g matrix as an interaction between the projectile and the nucleons in the target, whereas, on the other hand, to calculate nuclear structure, we consider effective interactions that have been separately adjusted. As long as we focus on studying medium energy scattering, one can find justifications for proceeding in this way. However, at low energy, this approach would be more questionable and it is likely that the derivation of an optical potential in the frame of a more fundamental theory (as in Ref. [42]) should be considered.

A. The mean-field approximation

The simplest description of the nuclear structure is provided by the self-consistent mean-field theory, that is also called Hartree-Fock (HF). There, the ground state is a Slater determinant constructed with individual particle states that are solutions of the HF equations. In this work, we use the HF results obtained using two different interactions. One is the Skyrme SkM* [37] interaction, and the other one is the finite-range, density-dependent D1S interaction [35]. The details of the HF formalism used with the D1S density-dependent interaction can be found in [43,44].

To calculate the one-body matrix elements $\rho_{\alpha\beta}$ of Sec. II, it is convenient to express the HF ground state in second quantization as

$$|HF\rangle = \prod_h a_h^+ |0\rangle. \tag{5}$$

The above product contains only occupied states labeled "h" (hole states) according to the usual terminology. The creation operator a_h^+ associated with the creation of a hole in a HF single particle state is defined with: $\varphi_h(r) = \langle r|a_h^+|0\rangle$, where $|0\rangle$ is the single particle vacuum.

By introducing these notations, the matrix elements $\rho_{\alpha\beta}$ read

$$\rho_{\alpha\beta} = \langle HF|a_\beta^+ a_\alpha|HF\rangle. \tag{6}$$

and are diagonal ($\rho_{h,h} = 1$, $\rho_{p,p} = 0$) in the HF approximation.

B. Description of the ground state beyond the HF approximation

The density-dependent effective interaction D1S has successfully been used in various extensions of the mean-field theory. Among them, the one of interest for our study is the microscopic description of collective excitations for closed shell nuclei as described in Ref. [36]. We recall some essential features of this approach and make the link with the usual RPA theory. This will permit us to define the two variants of correlated ground states that we propose for the description of the target.

1. Ground-state correlations induced by collective excitations

The approach of Ref. [36] is based on the quadratic form introduced to study the stability conditions of the HF solutions. It is obtained by performing a Taylor expansion of the energy E up to second order in the variation of the density matrix around the equilibrium HF density ($\rho^{(0)}$). The quadratic form in question is expressed in terms of the matrix

$$\begin{pmatrix} A & B \\ B^* & A^* \end{pmatrix}, \tag{7}$$

with elements

$$A_{(ph),(p'h')} = \delta_{pp'}\delta_{h,h'}(\epsilon_p - \epsilon_h) + \left(\frac{\partial^2 E/\partial\rho_{ph}}{\partial\rho_{p'h'}}\right)_{\rho=\rho^{(0)}}, \tag{8}$$

and

$$B_{(ph),(p'h')} = \left(\frac{\partial^2 E}{\partial\rho_{ph}\partial\rho_{h'p'}}\right)_{\rho=\rho^{(0)}}, \tag{9}$$

where ϵ_p and ϵ_h are the HF single-particle energies for a particle state and a hole state, respectively. This matrix is used to define a set of RPA equations [36,45], namely

$$\begin{pmatrix} A & B \\ B^* & A^* \end{pmatrix}\begin{pmatrix} X \\ Y \end{pmatrix} = \omega\begin{pmatrix} X \\ -Y \end{pmatrix}, \tag{10}$$

where ω is a set of eigenvalues corresponding to a set of eigenvectors with components X and Y. The definition of the matrix (7) presents the advantage to show that, because of its explicit dependence on the density, the particle-hole matrix elements of D1S must contain the so-called rearrangement terms in addition to the usual ones. Notice also that one retrieves the usual particle-hole matrix elements when the interaction does not depend on the density. Once such prescription is adopted for defining the particle-hole vertices, the approach developed in Ref. [36] follows closely the standard RPA theory as described extensively in Ref. [45]. Below we only give the relevant definitions that introduce the quantities of interest for this work. We express the formalism in a representation that accounts for rotational invariance and reflection symmetries of the nuclear interaction and the mean field as well (see Appendix A). Creation and annihilation operators are defined through a Bogolyubov transformation

$$\begin{aligned} \Theta^+_{i,(\pi,J,M)} &= \sum_{p,h} X^{\pi,J}_{i,(p,h)} A^+_{(p,h)}(\pi, J, M) \\ &\quad + Y^{\pi,J}_{i,(p,h)} \bar{A}_{(p,h)}(\pi, J, M), \\ \bar{\Theta}_{i,(\pi,J,M)} &= \sum_{p,h} Y^{\pi,J}_{i,(p,h)} A^+_{(p,h)}(\pi, J, M) \\ &\quad + X^{\pi,J}_{i,(p,h)} \bar{A}_{(p,h)}(\pi, J, M), \end{aligned} \tag{11}$$

which mixes the creation and destruction operators, $A^+_{(p,h)}(\pi, J, M)$ and $\bar{A}_{(p,h)}(\pi, J, M)$ respectively, of independent particle-hole pairs with definite angular momentum and

parity. The amplitudes X and Y are the components of the solutions of the RPA equations defined in Eq. (10). Because we work within the quasiboson approximation, the Bogolyubov transformation is nothing but a canonical transformation between two sets of bosons. Excitation modes of the nucleus are then defined through the action of any creation operator Θ^+ onto the quasiboson vacuum $|\tilde{0}\rangle$ of the destruction operator Θ. This is expressed as follows:

$$\begin{aligned} |i,(\pi,J,M)\rangle &= \Theta^+_{i,(\pi,J,M)}|\tilde{0}\rangle, \\ \Theta_{i,(\pi,J,M)}|\tilde{0}\rangle &= 0 \quad \forall i,\pi,J,M. \end{aligned} \tag{12}$$

The quasiboson vacuum can be constructed explicitly from the vacuum $|HF\rangle$ of the $A_{(p,h)}(\pi,J,M)$ operators. According to Ref. [45] it reads

$$|\tilde{0}\rangle = Ne^{\hat{Z}}|HF\rangle, \tag{13}$$

with

$$\hat{Z} = \frac{1}{2}\sum_{\pi,J}\sum_{(ph),(p'h')} Z^{\pi,J}_{(ph),(p'h')}[A^+_{(p,h)}(\pi,J)\otimes A^+_{(p',h')}(\pi,J)]^0_0,$$

and the normalization N defined as

$$N = \langle HF|\tilde{0}\rangle.$$

This form shows clearly that the quasiboson vacuum is a superposition of (2p-2h), 2 (2p-2h)... n (2p-2h) excitations coupled to zero angular momentum as it should, because the total spin of the ground state is zero for the nuclei under consideration. In the present work and for future applications to inelastic scattering we assume that the quasiboson vacuum [Eq. (13)] and the excited modes [Eq. (12)] provide a reasonable description of the ground state and nuclear excitations of the target.

At this stage it is worth pointing out that there exists another explicit form of the correlated ground state that has been derived [25] by summing up the RPA diagram to all orders. This important work shows that the resulting ground state, denoted here as $|RPA\rangle$, has exactly the same structure as the quasiboson vacuum, but it reveals also that the quasiboson counts twice the lowest-order term of the perturbation theory. How it affects mean values of one body operator is now shown on the matrix elements of the one-body density operator.

2. *One-body density matrix for the RPA ground state*

The one-body density matrix calculated in correlated ground states is no longer diagonal but contains all the elements of the form $\rho_{h,h'}$ and $\rho_{p,p'}$. The nondiagonal particle-hole matrix elements vanish because of the structure of the ground state. Moreover, on the account of symmetries it can be shown that the density matrix reduces to diagonal block matrices labeled by (l,j,τ) and independent of the projection m of the angular momentum j, namely

$$\rho_{(\alpha),(\beta)} = \delta_{l_\alpha,l_\beta}\ \delta_{j_\alpha,j_\beta}\ \delta_{\tau_\alpha,\tau_\beta}\ \rho_{(n_\alpha,l_\alpha,j_\alpha,\tau_\alpha),(n_\beta,l_\alpha,j_\alpha,\tau_\alpha)}. \tag{14}$$

Finally, it is often convenient in the formalism to perform the summation over m in advance and to consider the following quantities instead

$$\bar{\rho}_{(\alpha),(\beta)} = \sum_m \rho_{(\alpha),(\beta)} = (2j_\alpha+1)\rho_{(\alpha),(\beta)}. \tag{15}$$

We next provide expressions for these quantities in the cases of the quasiboson vacuum and RPA vacuum

$$\begin{aligned} \bar{\rho}_{(\alpha),(\beta)} &= \langle\tilde{0}|\sum_m a^+_{(\beta)}a_{(\alpha)}|\tilde{0}\rangle, \\ \bar{\rho}^{\rm RPA}_{(\alpha),(\beta)} &= \langle{\rm RPA}|\sum_m a^+_{(\beta)}a_{(\alpha)}|{\rm RPA}\rangle. \end{aligned} \tag{16}$$

The calculation in the quasiboson vacuum is straightforward. We give the result only for the particle and hole cases, respectively, as follows:

$$\bar{\rho}_{(\alpha),(\beta)} = \delta_{(\alpha),(\beta)}\sum_{i,J,\pi,h}(2J+1)Y^{\pi,J}_{i,(\alpha,h)}Y^{\pi,J}_{i,(\beta,h)}\delta_{\tau_h,\tau_\alpha}, \tag{17}$$

and

$$\bar{\rho}_{(\alpha),(\beta)} = \delta_{(\alpha),(\beta)}\left[\delta_{n_\alpha,n_\beta} - \sum_{i,J,\pi,h}(2J+1)Y^{\pi,J}_{i,(\alpha,h)}Y^{\pi,J}_{i,(\beta,h)}\delta_{\tau_h,\tau_\alpha}\right],$$

with the definition $\delta_{(\alpha),(\beta)} = \delta_{l_\alpha,l_\beta}\delta_{j_\alpha,j_\beta}\delta_{\tau_\alpha,\tau_\beta}$.

To calculate the RPA one-body matrix elements one refers to Ref. [24], where expressions of the occupation probabilities of single-particle orbitals in the RPA state can be found. Although such probabilities involve only diagonal matrix elements of the density, it is not difficult to generalize an expression for the nondiagonal ones. It turns out that the one-body matrix elements in the RPA state and those in the quasiboson vacuum [Eq. (17)] differ only by the lowest-order contribution in the perturbation theory. The correction terms are given for particle and hole cases, respectively, as

$$\begin{aligned} \Delta\bar{\rho}_{(\alpha),(\beta)} = -\frac{1}{2}\delta_{(\alpha),(\beta)}&\sum_{J,\pi}(2J+1) \\ &\times\sum_{p',h',h}\frac{B^{\pi,J}_{(\alpha,h),(p',h')}B^{\pi,J}_{(\beta,h),(p',h')}\delta_{\tau_\alpha,\tau_h}}{[\epsilon_{(p',h')}+\epsilon_{(\alpha,h)}][\epsilon_{(p',h')}+\epsilon_{(\beta,h)}]}, \end{aligned} \tag{18}$$

and

$$\begin{aligned} \Delta\bar{\rho}_{(\alpha),(\beta)} = -\frac{1}{2}\delta_{(\alpha),(\beta)}&\sum_{J,\pi}(2J+1) \\ &\times\sum_{p,p',h'}\frac{B^{\pi,J}_{(p,\alpha),(p',h')}B^{\pi,J}_{(p,\beta),(p',h')}\delta_{\tau_\alpha,\tau_p}}{[\epsilon_{(p',h')}+\epsilon_{(p,\alpha)}][\epsilon_{(p',h')}+\epsilon_{(p,\beta)}]}, \end{aligned}$$

where the $\epsilon_{(p,h)} = \epsilon_p - \epsilon_h$ are the free particle-hole pair energies and $B^{\pi,J}_{(p,h),(p',h')}$ the values defined in Eq. (9) for particle-hole pairs with good angular momentum J and parity π. With these notations, the RPA density matrix reads as follows:

$$\bar{\rho}^{\rm RPA}_{(\alpha),(\beta)} = \bar{\rho}_{(\alpha),(\beta)} + \Delta\bar{\rho}_{(\alpha),(\beta)}. \tag{19}$$

This expression is folded with the Melbourne g matrix [see Eq. (2)] and the optical potential so obtained is then used to calculate elastic scattering observables.

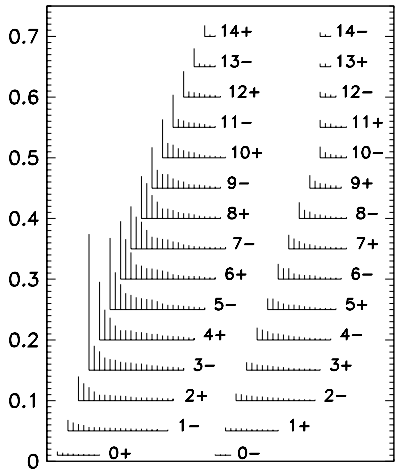

FIG. 1. Values of the quantities $\bar{\theta}_{\alpha}^{\pi,J}$ defined in the text. We present the contributions for ^{208}Pb, $\alpha = 1 \rightarrow 20$ first states of each (π, J) block.

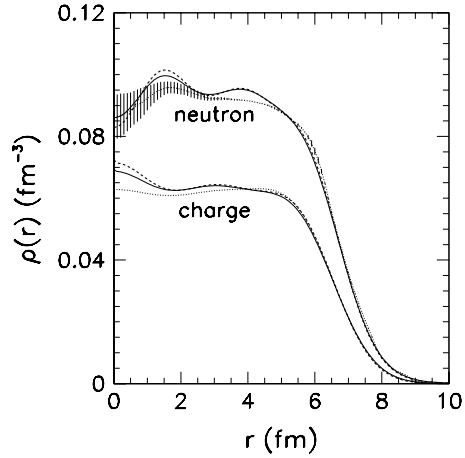

FIG. 2. Charge and neutron radial densities of ^{208}Pb. Comparisons between experimental data [46,47] (dotted curves), correlated (full curves) and uncorrelated (dashed curves) calculations.

3. Structure of correlated ground states

From inspection of the vacuum structure [Eq. (13)] as outlined in Appendix B, it is clear that the θ_{α} amplitudes [see Eq. (B3)] provide a direct measure of ground-state correlations. Taking into account the $(2J + 1)$-fold degeneracy of the θ_{α}s in each (π, J) subspace, the ratio

$$\bar{\theta}_{\alpha}^{\pi,J} = \frac{(2J+1)}{(2J_{\mathrm{Ref}}+1)}\theta_{\alpha}^{\pi,J}, \tag{20}$$

is a measure of the relative importance of each subspace, with J_{Ref} taken as the multipolarity of the one that provides the main contribution to the overall correlations (here, $J_{\mathrm{Ref}} = 3$). These ratios shown in Fig. 1 for ^{208}Pb indicate that some natural and unnatural parity states of all (π, J) subspaces, even high-spin ones, are worthy of consideration for building the correlated ground state.

As the correlations are smearing out the occupation probability distribution of proton and neutron single-particle levels around their respective Fermi energies, the radial ground state densities get depleted toward the nuclear center. This effect can be seen in Fig. 2 where measured charge and neutron distributions are shown together with our HF and HF+RPA predictions for ^{208}Pb. Calculated root-mean-square (rms) radii of proton, charge, and neutron distributions as well as neutrons skins are gathered in Table I for ^{208}Pb as well as for ^{16}O, ^{40}Ca, and ^{48}Ca. A good overall agreement between the RPA predictions and experimental values is obtained.

IV. ANALYSES OF SCATTERING OBSERVABLES

To test the predictions of the OMP described above, an incident proton experimental database was built, comprising differential cross sections $\sigma(\theta)/\sigma_{\mathrm{Ruth}}$, analyzing powers $A_y(\theta)$ and spin rotation functions $R(\theta)$ and $Q(\theta)$. References to these data are provided in Table II only for ^{208}Pb. The incident energies of present interest are limited to the 40–201 MeV range where the Melbourne OMP is most successful [31]. For all the comparisons between model predictions and experimental data shown below the continuous and dashed curves represent the OMP calculations based on one-body density matrix elements of correlated (RPA) and uncorrelated ground states (HF), respectively.

A. Incident protons

Proton scattering experiments have provided a wealth of valuable information on angular distributions for various observables at many incident energies. For this reason, the proton database we have formed in Table II serves as the main playground for detailed OMP analyses. We also show some illustrations for the three other stable doubly closed-shell nuclei ^{16}O, ^{40}Ca, and ^{48}Ca.

1. ^{208}Pb

The differential cross sections discussed below are normalized to Rutherford scattering cross sections to magnify differences existing between our OMP predictions and scattering data. This comparison is shown in the upper panel of Fig. 3. Similar comparisons for $A_y(\theta)$ are shown in the lower panel of Fig. 3.

For the comparison between solid (RPA-based) and dashed (HF-based) curves for cross sections, it turns out that the former is systematically lower over most scattering angles. Compared to OMP predictions based on the Hartree-Fock ground-state density matrix, those using the RPA one are all in closer agreement with the spread of cross-section data except at lower incident energies where the calculated minima seem too deep. This is a known low-energy shortcoming of the g-folding model that has been noticed previously [64]. Nevertheless, the agreement between RPA-based calculations and measured differential cross sections is good, especially at the higher incident energies, where HF- and RPA-based calculations differ the most, and considering that no parameter was adjusted.

Extending the comparison from experimental cross sections to analyzing powers, it may be seen in the lower part of

TABLE I. Proton, charge, and neutron rms radii for ^{16}O, ^{40}Ca, ^{48}Ca, and ^{208}Pb. Comparisons between present HF and HF+RPA predictions, and experimental values . The neutron skin $\Delta r_{\rm np}$ is defined as $\Delta r_{\rm np} = \langle r_n^2\rangle^{1/2} - \langle r_p^2\rangle^{1/2}$. The estimated $\langle r_n^2\rangle^{1/2}$ and $\Delta r_{\rm np}$ values of Refs. [49,50] are from systematics.

Nucleus		$\langle r_p^2\rangle^{1/2}$ (fm)	$\langle r_{\rm ch}^2\rangle^{1/2}$ (fm)	$\langle r_n^2\rangle^{1/2}$ (fm)	$\Delta r_{\rm np}$ (fm)
	Exp		2.730(25) [48]		
^{16}O	HF	2.669	2.718	2.647	−0.022
	HF+RPA	2.658	2.728	2.678	−0.020
					−0.040 [50]
	Exp		3.482(25) [48]	3.312(2) [49]	
					−0.065(2) [49]
^{40}Ca	HF	3.408	3.470	3.365	−0.043
	HF+RPA	3.421	3.483	3.381	−0.040
					+0.128 [50]
	Exp		3.470(9) [48]	3.436(23) [49]	
					+0.079(23) [49]
^{48}Ca	HF	3.441	3.496	3.588	+0.144
	HF+RPA	3.455	3.510	3.590	+0.130
					+0.15(2) [50]
	Exp		5.503(7) [48]	5.511(11) [49]	+0.12(7) [51]
					+0.097(14) [49]
^{208}Pb	HF	5.432	5.475	5.567	+0.135
	HF+RPA	5.467	5.504	5.592	+0.125

Fig. 3 that the correlated ground-state specifications lead to a excellent overall OMP description of the $A_y(\theta)$ data spread, especially at medium angles for energies E $\geqslant$ 150 MeV. A similar statement is made for the spin-rotation functions $R(\theta)$ and $Q(\theta)$ measured at 65 and 201 MeV, respectively. As can be seen in Fig. 4 the phasing and amplitude of these measured observables are well accounted for by our OMP calculations, although these observable predictions do not seem very sensitive to RPA correlations.

The increasing mismatch between experimental data and calculations as incident energies decrease is most likely related to effects that are outside the g matrix derivation. These effects stem from particle-phonon couplings that give rise to a second-order component (Feshbach term) in the optical model potential [65–68]. A full calculation of medium energies OMPs should include both (and avoid double counting) the g matrix and the Feshbach components whose relative weights are expected to change from low to high incident energies. Thus, the disagreements between our pure g-matrix calculations and data can be seen as a measurement of the effects of the neglected collective inelastic channel contributions. Those effects become sizable below 60 MeV, the region where collective excitations are expected to take place in nuclei. Contributions from inelastic channels result in an increase in the imaginary component of the OMP. To estimate the amplitude of the the imaginary OMP correction needed to account for the experimental data at 40 MeV, a sensitivity calculation was performed showing that an upward renormalization of the imaginary OMP component of the order of 25% is necessary to account for the back angles data. We can thus conclude that the changes to the imaginary component of the OMP induced by the coupling to collective states are very sizable at low energies and that an optical model containing only g-matrix components is more suited to describing scattering at energies greater than 60 MeV.

TABLE II. $\sigma(\theta)/\sigma_{\rm Ruth}$, $A_y(\theta)$, $R(\theta)$, and $Q(\theta)$ database for proton scattering off ^{208}Pb.

Energy (MeV)	Ref.	Energy (MeV)	Ref.
40	[52]	104.4,121.2	[53]
45,47.3	[54]	156	[55]
61.4	[56]	160	[57]
65	[58]	182.4	[53]
79.9	[53]	185	[59]
97	[59]	201	[60–63]

2. Other doubly magic nuclei

Calculations were also performed for protons incident on the other stable doubly magic nuclei ^{16}O, ^{40}Ca, and ^{48}Ca. Although these calculations were performed for all incident energies where experimental data are available, Fig. 5 only displays comparisons at highest energies, where the difference between HF- and HF+RPA-based OMPs is the most striking. Those results are representative of the agreement obtained over the range from 60 to 201 MeV. For these doubly magic nuclei, comparison between calculations using correlated and uncorrelated ground-state density matrices, and the experimental data, allows us to confirm the conclusions of

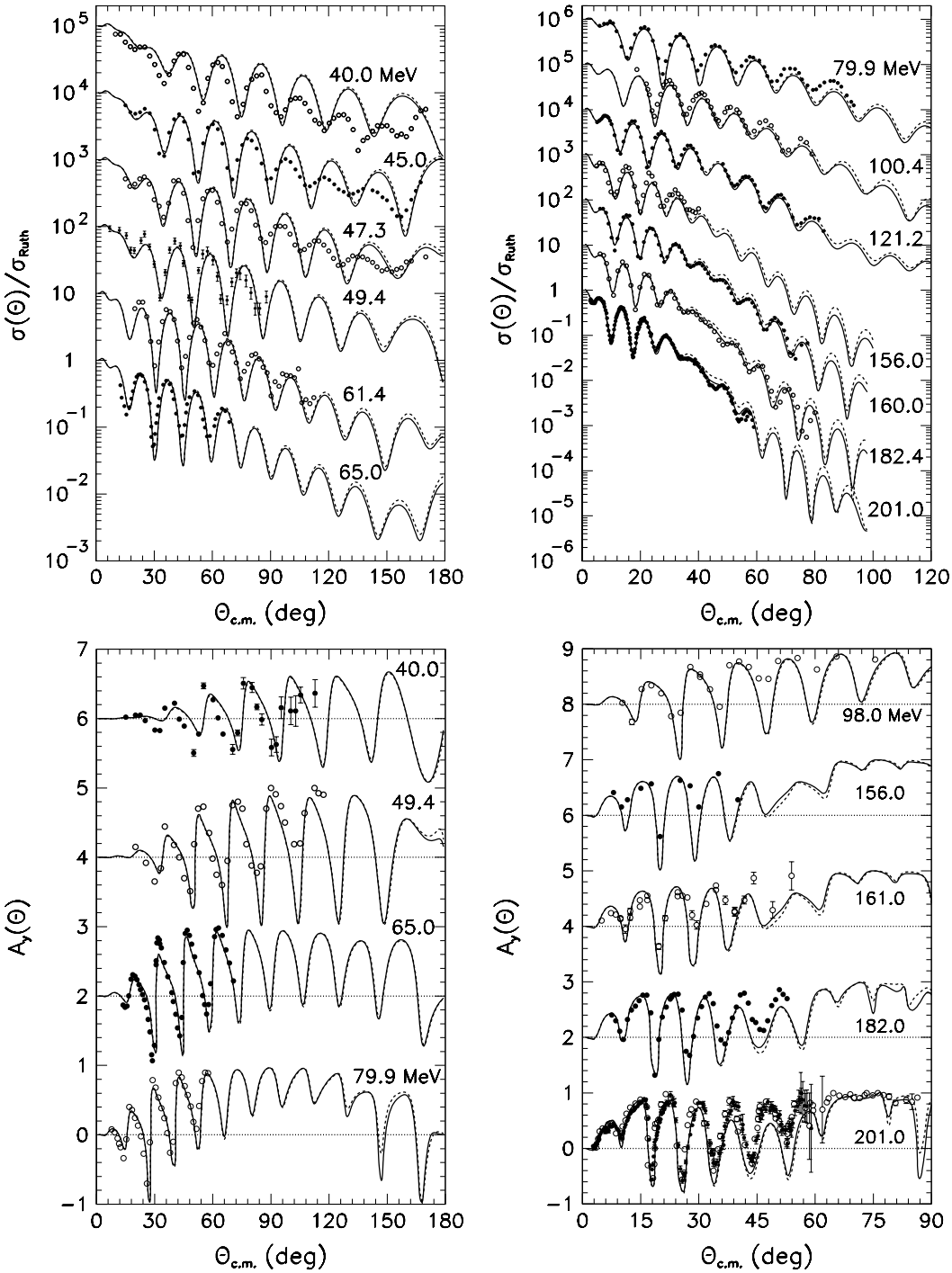

FIG. 3. Differential cross sections $\sigma(\theta)/\sigma_{\rm Ruth}$ and analyzing powers $A_y(\theta)$ for protons incident on ^{208}Pb. Comparison between data (symbols) and OMP predictions based on correlated (solid curves) and uncorrelated (dashed curves) descriptions of the ground state. Cross sections are offset by factors 10, whereas analyzing powers are shifted by 2.

the $\vec{p} + {}^{208}$Pb scattering study with a larger data sample. Below 60 MeV, our predictions exhibit deficiencies similar to those encountered for lead.

B. Incident neutrons

Although some neutron scattering data is available [69–71] at neutron energies higher than 40 MeV, those data sets (with the notable exceptions of Refs. [70,71]) do not extend far enough in angles to allow for discrimination between the nuclear structure models used as a basis for our OMP analyses. Thus, those data sets can be described in a satisfactory way above 60 MeV by our OMP using either the HF or RPA one-body density matrix. Moreover, when comparing incident proton and incident neutron calculations, no effect specific to incident neutrons was observed, and as for incident protons, the

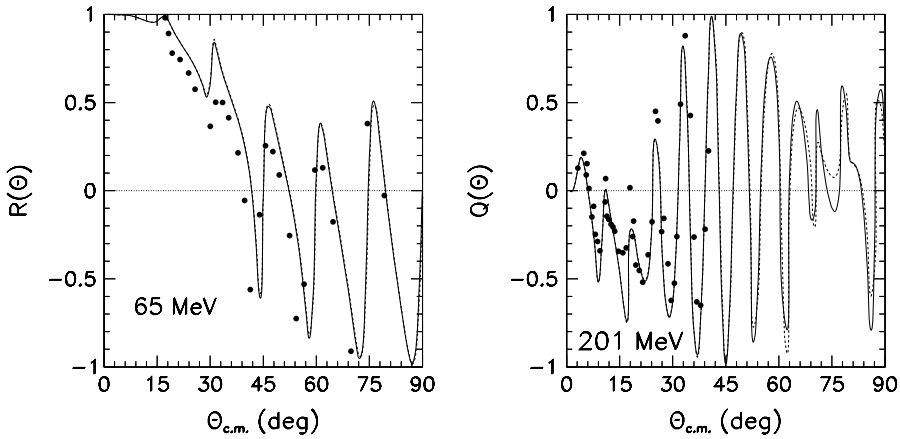

FIG. 4. Spin rotation functions $R(\theta)$ and $Q(\theta)$ at 65 and 201 MeV for protons incident on ^{208}Pb. Comparisons between experimental data (symbols) and present OMP calculations for correlated (solid curves) and uncorrelated (dashed curves) ground state descriptions.

RPA-based neutron-nucleus OMP calculations predict cross sections that are systematically lower at large angles than their HF counterparts. Nevertheless, the scarcity of high-energy, large angular range neutron scattering data calls for new measurements of the quality of those in Refs. [70,71], may be at higher energy.

We conclude these analyses with making the statement that the RPA correlations have sizable impacts on the OMP predictions only at the higher incident energies of present interest and for center-of-mass scattering angles larger than typically $\theta \sim 30^\circ$. This statement is relevant to ^{16}O, ^{40}Ca, ^{48}Ca, and ^{208}Pb target nuclei. This statement should, however, be moderated by the fact that the pure g-matrix treatment of the OMP used here does not take into account the coupling to collective states that becomes important at low ($E < 60$ MeV) projectile energies.

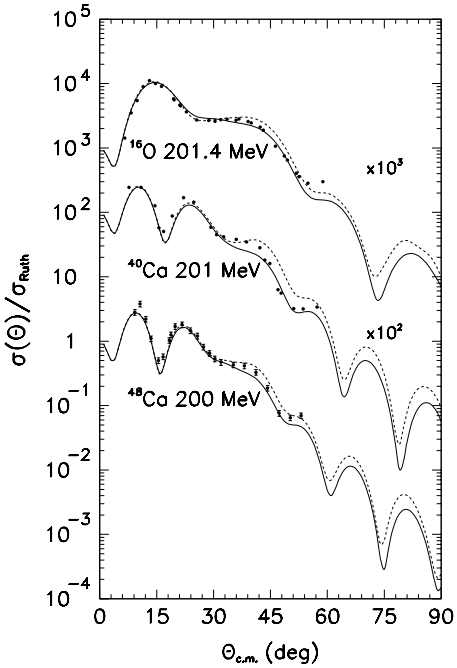

FIG. 5. Differential cross sections $\sigma(\theta)/\sigma_{\text{Ruth}}$ for protons incident on ^{16}O, ^{40}Ca, and ^{48}Ca. Comparison between experimental data (symbols) and OMP predictions based on correlated (solid curves) and uncorrelated (dashed curves) descriptions of the ground state. Cross sections offset factors and proton incident energies are indicated on the figure. Data are taken from Ref. [72] for ^{16}O and ^{40}Ca and from Ref. [73] for^{48}Ca.

C. Discussion

As discussed in Sec. IV A 1, we have seen evidence that the g-matrix approach to the OMP is more relevant for the higher part of our incident energy range, where effects of coupling to collective states produce negligible corrections to the g-matrix treatment. For this reason the following discussion focuses only on the higher energy range (60–200 MeV), where our physical conclusions will not be affected by the absence of proper treatment of coupling to collective states.

1. Probing ground-state correlations

In Sec. IVA, we have shown that similarly to electron scattering, nucleon scattering is sensitive to small details of the nuclear structure of the target nuclei, such as those stemming from the presence of long-range correlations in the target ground state. Moreover, including such correlations does improve the agreement between calculated and measured scattering cross sections. Next comes the difficult question of identifying the features of the correlated density matrix that nucleon scattering is sensitive to. Looking at Fig. 3 can provide us with hints to that effect: the differences between HF- and RPA-based calculations can be seen to be stronger at large angles, suggesting that such differences appear when more interior regions of the target are probed. Replotting the $p+^{208}$Pb scattering cross sections as functions of the momentum transfer q (see Fig. 6) confirms that, indeed, for all energies, differences between HF- and RPA-based calculations are associated with values of q larger than 1.7 fm^{-1} and thus deeper regions of the target. Figure 2 displays the radial charge density of ^{208}Pb calculated with (solid curve) and without (dashed curve) RPA correlations in the ground state, showing the well-known effect of RPA correlations, i.e., depleting the interior of the density distributions and enlarging the distributions rms radii. The fact that only $q \geqslant 1.7$ fm^{-1} cross sections are impacted by RPA correlations suggests that this value of the momentum transfer constitutes the threshold above which the depletion of the probed inner surface regions of the

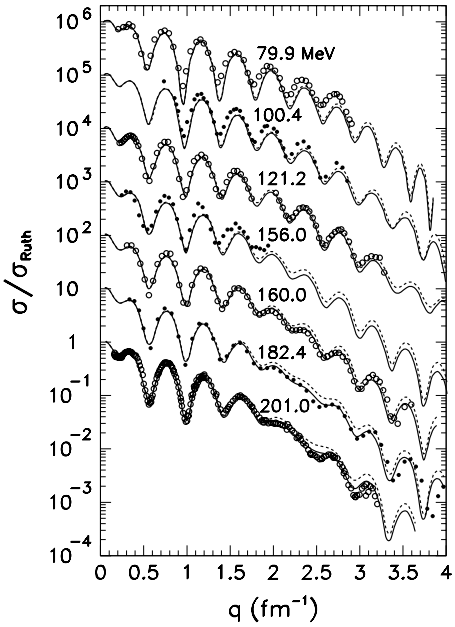

FIG. 6. Proton elastic scattering from ^{208}Pb: differential cross sections $\sigma/\sigma_{\rm Ruth}$ as functions of the momentum transfer q. For more details, see the legend to Fig. 3.

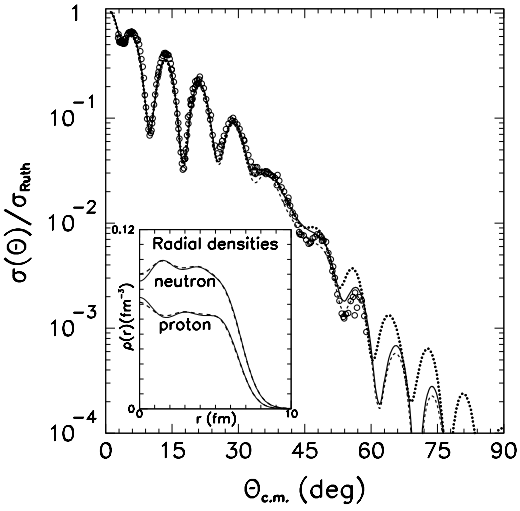

FIG. 7. Differential cross sections $\sigma(\theta)/\sigma_{\rm Ruth}$ for 201 MeV protons incident on ^{208}Pb. Comparison between experimental data (symbols) and OMP predictions based on correlated (solid curves), correlated without double counting corrections (dashed curves), and Hartree-Fock SkM* (dotted curve) descriptions of the ground state. The insert shows comparison between proton and neutron radial densities for correlated (solid curves) and correlated without double counting corrections (dashed curves) descriptions of the ground state.

target becomes sizable. Because of the absorption, the interior region of the target cannot be probed. However, because the density matrix used as an input to our microscopic OMP calculations conveys much more complex nuclear structure information than does the radial density alone, disentangling the effects of the RPA correlations on nucleon scattering is a much more difficult task than analyzing the q dependence of the radial density. Therefore, unlike the case of electron scattering, such an analysis can at best provide qualitative insight into the actual sensitivity of nucleon scattering to the presence of RPA correlations in the one-body density matrix of the target.

2. Double counting

Further tests of the sensitivity of our scattering predictions to changes in matter distributions have been performed by ignoring the $\Delta\rho$ double counting correction terms [see Eqs. (18) and (19)]. Elastic scattering calculation results performed with (solid curve) and without (dashed curve) these correction terms are shown in Fig. 7 for 201-MeV protons incident on ^{208}Pb. First, Fig. 7 shows that including or ignoring the $\Delta\rho$ correction produces nonnegligible changes in the calculated scattering cross section. Moreover, except for a local improvement at $\theta = 54^\circ$ over those using $\Delta\rho \neq 0$ (solid curve), the agreement between data and the OMP calculation with $\Delta\rho = 0$ is worse all over the range $\theta \geqslant 34^\circ$. Setting $\Delta\rho$ to 0 leads to increasing the rms radii from $\langle r^2_{\rm ch}\rangle^{1/2} = 5.504$ fm ($\Delta\rho \neq 0$, see Table I) to $\langle r^2_{\rm ch}\rangle^{1/2} = 5.517$ fm ($\Delta\rho = 0$), a value falling apart from the experimental result $\langle r^2_{\rm ch}\rangle^{1/2} = 5.503(7)$ fm (see Table I). The ^{208}Pb neutron and proton radial shapes calculated assuming $\Delta\rho = 0$ (dotted curves) and $\Delta\rho \neq 0$ (full curves) are shown in the insert of Fig. 7. The above discussion shows that the $\Delta\rho$ double counting correction to the RPA density matrix should not be ignored in scattering calculations.

3. Skyrme Hartree-Fock model

In recent years, Skyrme Hartree-Fock models have been considered to assess the neutron rms radius in ^{208}Pb [74]. Furthermore, various Skyrme force parametrizations have been tested in NA g-folding model calculations to discern which one provides the best representation of the neutron density. As a result, it turns out that SkM* seems appropriate when combining analyses of electron and nucleon scattering data. g-folding model calculations with HF/SkM* as input have again been performed and compared with calculations based on the present correlated ground-state densities. The comparison made for (p, p) scattering off ^{208}Pb at 201 MeV is shown in Fig. 7 where the dotted and solid curves are for results from the HF/SkM* and HF+RPA/D1S based OMPs, respectively. The dotted and solid curve overlap each other over most of the angular range, except perhaps for angles above 50°. This is not surprising because both HF/SkM* and HF+RPA/D1S structure calculations provide nearly identical radial matter distributions and neutron skins for ^{208}Pb. However, this similarity conceals more fundamental differences: whereas the SkM* interaction was designed to reproduce the measured charge radii of many stable nuclei within the HF framework only (its parameters take care of correlations present in nuclear ground states in an effective way at the mean-field level), the D1S interaction is designed not to include such correlation effects in its parametrization, so that correlations can be explicitly taken care of, in a detailed way, at a level that goes beyond that of the mean-field approximation.

V. CONCLUSIONS

We present a comprehensive analysis of ground-state structure properties of doubly closed-shell nuclei, together with the impacts they have on the interpretation of nucleon elastic scattering observables within the Melbourne *g*-folding model. Long-range correlations are treated in the self-consistent RPA theory implemented with the D1S force, and the long-standing problem relevant to double counting is solved to calculate local and nonlocal densities. The theoretical framework that in the past proved successful in the interpretation of electron scattering measurements is shown to be equally successful in the analyses of nucleon elastic scattering between 60 and 201 MeV. All the measured differential cross sections, analyzing powers and spin-rotation functions are well described, *with no adjusted parameter*. Turning off RPA correlations (or not implementing them properly, i.e., without considering double counting corrections) negatively affects the agreement between experimental data and calculations, an effect that becomes more and more sizable as incident energy and momentum transfer increase. It seems plausible that the differences observed between predictions are strongly tied to differences between correlated and uncorrelated matter densities only in the outer and inner surface regions.

Another important lesson that can be learned from the present study is related to the validity of a pure *g*-matrix approach of the OMP as a function of projectile energies. Whereas at high energies pure *g* matrix seems to be satisfactory as far as reproducing elastic scattering data is considered, at lower energies ($E < 60$ MeV), the disagreement between measured and calculated elastic scattering cross sections becomes sizeable. We attribute that disagreement to the components of the OMP that are not included in the *g* matrix: the coupling to collective excitations of the target. Indeed a 25% renormalization of the imaginary OMP would be needed to account for the 40 MeV experimental data at the back angles. Although a study of the OMP, including both the *g* matrix and coupling to collective excitation components (also avoiding double counting) is outside the scope of the present article, our work highlights the necessity of such a treatment for projectile energies around 40 MeV, where none of those two components dominate. On the other hand, for energies between 60 and 200 MeV, the *g*-matrix component seems to be dominant, and conversely, the effect of coupling to collective states can be neglected (or more precisely mostly reduces to the *g*-matrix component which is already included). In this energy range, the Melbourne *g* matrix produces a good approximation of the "true" OMP and can be used as a tool to probe details of the nuclear structure of the target.

Finally, because in RPA theory the correlated ground state happens to be the vacuum on which excited states are built as quasibosons excitations, a framework is at hand for extending our *g*-folding model analyses from elastic scattering to inelastic scattering from low to high excitation energy levels. Work along this line is in progress.

ACKNOWLEDGMENTS

We acknowledge the usefulness of discussions with S. Peru on the RPA formalism and codes. We are also deeply indebted to J. Raynal for his relentless support of his microscopic DWBA code and for invaluable insights into many obscure but nevertheless very important points.

APPENDIX A: DEFINITION

The Hartree-Fock solutions in the spherical case take the form

$$\langle x|(nlj), m, \tau\rangle = R^{\tau}_{nl}(r) i^{l} [\chi^{1/2}(\sigma) \otimes Y^{l}(\Omega)]^{j}_{m} \chi^{1/2}(\tau). \quad \text{(A1)}$$

The operator $a^{+}_{(nlj),m,\tau}$ creates a particle in this state and its hermitian conjugate defines the destruction operator $a_{(nlj),m,\tau}$. It is convenient to define destruction operators $\bar{a}_{(nlj),m,\tau}$ through the relation

$$\bar{a}_{(nlj),m,\tau} = (-)^{j+m} a_{(nlj),-m,\tau}. \quad \text{(A2)}$$

Indeed, with this definition, both $a^{+}_{(nlj),m,\tau}$ and $\bar{a}_{(nlj),m,\tau}$ transform under rotations such as the component m of an irreducible tensor of rank j. Consequently creation operators of particle-hole pairs of definite angular momentum are readily constructed with the usual rules for coupling two tensors:

$$\begin{aligned} A^{+}_{(p,h)}(\pi, J, M) &= [a^{+}_{(p),\tau} \otimes \bar{a}_{(h),\tau}]^{J}_{M} \\ &= \sum_{m_p, m_h} C^{j_p \; j \; J}_{m_p m_h M} \, a^{+}_{(p),m_p,\tau} \, \bar{a}_{(h),m_h,\tau}. \end{aligned} \quad \text{(A3)}$$

The parity π of the particle-hole pair that we indicate explicitly is defined by: $\pi = (-)^{l_p - l_h}$. As we did for the fermions, we define operators $\bar{A}$

$$\bar{A}_{(p,h)}(\pi, J, M) = (-)^{J-M} A_{(p,h)}(\pi, J, -M), \quad \text{(A4)}$$

which annihilate particle-hole pairs of angular momentum J and projection M. As a consequence, by mixing A^{+} and $\bar{A}$, the Bogolyubov transformation defines operators Θ^{+} and Θ, which respectively create and annihilate collective modes of definite angular momentum and parity. Finally, let us also recall that we consider only neutron and proton particle-hole pairs and consequently $\tau_p = \tau_h$.

APPENDIX B: THE QUASIBOSON VACUUM

The expression of the quasiboson vacuum takes a very simple form in the so-called canonical representation defined as follows

$$\begin{aligned} B^{+}_{\alpha}(\pi, J, M) &= \sum_{(ph)} D^{\pi,J}_{\alpha,(ph)} A^{+}_{(ph)}(\pi, J, M), \\ \bar{B}_{\alpha}(\pi, J, M) &= \sum_{(ph)} D^{\pi,J}_{\alpha,(ph)} \bar{A}_{(ph)}(\pi, J, M). \end{aligned} \quad \text{(B1)}$$

The transformation D is an orthogonal transformation that mixes separately the creation and destruction operators of the original particle-hole pairs (it is orthogonal because our Bogolyubov transformation is real). It is defined by solving the eigenvalues problem

$$\begin{aligned} \sum_{(p'h')} [\tilde{Y}^{\pi,J} Y^{\pi,J}]_{(ph),(p'h')} D^{\pi,J}_{\alpha,(p'h')} &= \rho^{\pi,J}_{\alpha} D^{\pi,J}_{\alpha,(ph)}, \\ [\tilde{Y}^{\pi,J} Y^{\pi,J}]_{(ph),(p'h')} &= \sum_{i} Y^{\pi,J}_{(ph)} Y^{\pi,J}_{(p'h')}. \end{aligned} \quad \text{(B2)}$$

In this representation, the vacuum reads

$$|\tilde{0}\rangle = \prod_{\pi,J}\left(\prod_{\alpha} \mathrm{ch}\,\theta_{\alpha}^{\pi,J}\right)^{(2J+1)} e^{\hat{Z}}|HF\rangle,$$

with

$$\hat{Z} = \frac{1}{2}\sum_{\pi,J,\alpha} \mathrm{th}\,\theta_{\alpha}^{\pi,J} \sum_{M} B_{\alpha}^{+}(\pi, J, M)\bar{B}_{\alpha}(\pi, J, M)$$
$$= \frac{1}{2}\sum_{\pi,J,\alpha} \mathrm{th}\,\theta_{\alpha}^{\pi,J}\,\hat{J}[B_{\alpha}^{+}(\pi, J)\otimes \bar{B}_{\alpha}(\pi, J)]_{0}^{0}. \quad \text{(B3)}$$

The angle $\theta_{\alpha}^{\pi,J}$ is related to the eigenvalues $\rho_{\alpha}^{\pi,J}$ through the relation:

$$\mathrm{th}\,\theta_{\alpha}^{\pi,J} = \sqrt{\frac{\rho_{\alpha}^{\pi,J}}{1+\rho_{\alpha}^{\pi,J}}}. \quad \text{(B4)}$$

This form shows clearly that the $\theta_{\alpha}^{\pi,J}$s provide a direct measure of the correlations that are induced by the RPA modes.

[1] J. M. Cavedon *et al.*, Phys. Rev. Lett. **49**, 978 (1982).
[2] E. N. M. Quint *et al.*, Phys. Rev. Lett. **57**, 186 (1986).
[3] E. N. M. Quint *et al.*, Phys. Rev. Lett. **58**, 1088 (1987).
[4] I. Sick and P. de Witts Huberts, Comments Nucl. Part. Phys. **20**, 177 (1991).
[5] V. R. Pandharipande and S. Pieper, Nucl. Phys. **A507**, 167 (1990).
[6] S. Fantoni and V. R. Pandharipande, Nucl. Phys. **A427**, 473 (1984).
[7] L. Lapikas, Nucl. Phys. **A553**, 297 (1993).
[8] S. C. Pieper, R. B. Wiringa, and V. R. Pandharipande, Phys. Rev. C **46**, 1741 (1992).
[9] J. H. Heisenberg and B. Mihaila, Phys. Rev. C **59**, 1440 (1999).
[10] I. Bobeldijk *et al.*, Phys. Rev. Lett. **73**, 2684 (1994).
[11] I. Bobeldijk *et al.*, Phys. Lett. **B353**, 32 (1995).
[12] V. R. Pandharipande, C. N. Papanicolas, and J. Wambach, Phys. Rev. Lett. **53**, 1133 (1984).
[13] V. R. Pandharipande, I. Sick, and P. K. deWitt Huberts, Rev. Mod. Phys. **69**, 981 (1997).
[14] R. Wiringa, Nucl. Phys. **A631**, 70c (1998).
[15] S. C. Pieper, V. R. Pandharipande, R. B. Wiringa, and J. Carlson, Phys. Rev. C **64**, 014001 (2001).
[16] R. B. Wiringa, S. C. Pieper, J. Carlson, and V. R. Pandharipande, Phys. Rev. C **62**, 014001 (2000).
[17] B. S. Pudliner, V. R. Pandharipande, J. Carlson, S. C. Pieper, and R. B. Wiringa, Phys. Rev. C **56**, 1720 (1997).
[18] S. Fantoni and V. R. Pandharipande, Phys. Rev. C **37**, 1697 (1988).
[19] V. Bernard and N. Van Giai, Nucl. Phys. **A348**, 75 (1980).
[20] C. Mahaux and R. Sartor, Nucl. Phys. **A493**, 157 (1989).
[21] C. Mahaux and H. Ngo, Nucl. Phys. **A431**, 486 (1984).
[22] C. Mahaux and R. Sartor, Nucl. Phys. **A546**, 65 (1992).
[23] C. Mahaux and R. Sartor, Adv. Nucl. Phys. **20**, 1 (1991).
[24] J. Dechargé and L. Sips, Nucl. Phys. **A407**, 1 (1983).
[25] J. Dechargé, L. Sips, and D. Gogny, Phys. Lett. **B98**, 229 (1981).
[26] H. Lenske and J. Wambach, Phys. Lett. **B249**, 377 (1990).
[27] D. Gogny, in *Lectures Notes in Physics*, edited by H. Arenhörel and Dreschel (Springer-Verlag, Berlin, 1979), Vol. 108, p. 88.
[28] Z. Y. Ma and J. Wambach, Phys. Lett. **B256**, 1 (1991).
[29] F. Petrovich, Nucl. Phys. **A354**, 499c (1981).
[30] W. Love, in *The (p,n) Reaction and the Nucleon-Nucleon Force* (Plenum, New York, 1980), p. 23.
[31] K. Amos, P. J. Dortmans, H. V. von Geramb, S. Karataglidis, and J. Raynal, Adv. Nucl. Phys. **25**, 275 (2000), and references therein.
[32] H. V. von Geramb, in *Lectures Notes in Physics*, edited by H. V. v. Geramb (Springer-Verlag, Berlin, 1978), Vol. 89, p. 104.
[33] P. Navratil and B. R. Barrett, Phys. Rev. C **57**, 3119 (1998).
[34] P. Schwandt, in *AIP Conference Proceedings*, edited by H. O. Meyer (Springer-Verlag American Institute of Physics, New York, 1983), Vol. 97, p. 89.
[35] J. F. Berger, M. Girod, and D. Gogny, Comput. Phys. Commun. **63**, 365 (1990), and references therein.
[36] J. Blaizot and D. Gogny, Nucl. Phys. **A284**, 429 (1977).
[37] J. Bartel, P. Quentin, M. Brack, C. Guet, and H.-B. Hakansoon, Nucl. Phys. **A386**, 79 (1982).
[38] R. Machleidt, K. Holinde, and C. Elster, Phys. Rep. **149**, 1 (1987).
[39] J. Raynal, computer code DWBA98, 1998, (NEA 1209/05).
[40] K. Amos, L. Canton, G. Pisent, J. P. Svenne, and D. van der Knijff, Nucl. Phys. **A728**, 65 (2003).
[41] L. Canton, G. Pisent, J. P. Svenne, D. van der Knijff, K. Amos, and S. Karataglidis, Phys. Rev. Lett. **94**, 122503 (2005).
[42] F. Villars, in *Fundamentals in Nuclear Theory: Collision Theory*, (IAEA, Vienna, 1967), p. 269.
[43] J. Dechargé and D. Gogny, Phys. Rev. C **21**, 1568 (1980).
[44] J. Dechargé, M. Girod, D. Gogny, and B. Grammaticos, Nucl. Phys. **A358**, 203c (1981).
[45] P. Ring and P. Schuck, *The Nuclear Many-Body Problem* (Springer-Verlag, New York, 1980).
[46] B. Frois, J. B. Bellicard, J. M. Cavedon, M. Huet, P. Leconte, P. Ludeau, A. Nakada, Phan Zuan Ho, and I. Sick, Phys. Rev. Lett. **38**, 152 (1977).
[47] V. E. Starodubsky and N. M. Hintz, Phys. Rev. C **49**, 2118 (1994).
[48] H. De Vries, C. W. De Jager, and C. De Vries, At. Data Nucl. Data Tables **36**, 495 (1987).
[49] B. C. Clark, L. J. Kerr, and S. Hama, Phys. Rev. C **67**, 054605 (2003).
[50] A. Trzcinska, J. Jastrzebski, P. Lubinsky, F. J. Hartmann, R. Schmidt, T. von Egidy, and B. Klos, Phys. Rev. Lett. **87**, 082501 (2001).
[51] M. Csatlos *et al.*, Nucl. Phys. **A719**, 304c (2003).
[52] L. N. Blumberg, E. E. G. A. van der Wende, A. Zucker, and R. H. Bassel, Phys. Rev. **142**, 812 (1966).
[53] A. Nadasen, P. Schwandt, P. P. Singh, W. W. Jacobs, A. D. Bacher, P. T. Debevec, M. D. Kaitchuck, and J. T. Meek, Phys. Rev. C **23**, 1023 (1981).
[54] W. T. H. Oers, H. Haw, N. E. Davison, A. Igemarsson, B. Stagerstrom, and G. Tibell, Phys. Rev. C **10**, 307 (1974).
[55] V. Comparat, R. Frascaria, N. Marty, M. Morlet, and A. Willis, Nucl. Phys. **A221**, 403 (1974).
[56] C. B. Fulmer, J. B. Ball, A. Scott, and M. L. Whiten, Phys. Rev. **181**, 1565 (1969).

[57] P. G. Ross and N. S. Wall, Phys. Rev. B **140**, 1237 (1965).
[58] H. Sakagushi, M. Nakamura, K. Hatakama, A. Goto, T. Noro, F. Ohtani, H. Sakamoto, H. Ogawa, and S. Kobayashi, Phys. Rev. C **26**, 944 (1982).
[59] P. Schwandt, H. O. Meyer, W. W. Jacobs, A. D. Bacher, S. E. Vigdor, M. D. Kaitchuck, and T. R. Donoghue, Phys. Rev. C **26**, 55 (1982).
[60] D. A. Hutcheon *et al*., in *Polarization Phenomena in Nuclear Physics*, Proceedings of the Fifth International Symposium on Polarization Phenomena in Nuclear Physics, Santa Fe, AIP Conf. Proc., No. 69, edited by G. G. Holsen, R. H. Brown, N. Jarnie, W. W. Mc Naughton, and G. M. Hale (AIP, New York, 1981), p. 454.
[61] M. Ju, M. S. thesis, Simon Fraser University, 1987.
[62] N. Ottenstein, S. J. Wallace, and J. A. Tjon, Phys. Rev. C **38**, 2272 (1988).
[63] L. Lee *et al*., Phys. Lett. **B205**, 219 (1988).
[64] P. K. Deb, K. Amos, and S. Karataglidis, Phys. Rev. C **62**, 037601 (2000).
[65] H. Feshbach, Ann. Phys. (NY) **5**, 357 (1958).
[66] H. Feshbach, Ann. Phys. (NY) **19**, 287 (1962).
[67] C. Rao, M. Reeves, and G. Satchler, Nucl. Phys. **A207**, 182 (1973).
[68] N. Vinh Mau and A. Bouyssy, Nucl. Phys. **A257**, 189 (1976).
[69] J. H. Osborne *et al*., Phys. Rev. C **70**, 054613 (2004).
[70] J. Klug *et al*., Phys. Rev. C **67**, 031601(R) (2003).
[71] J. Klug *et al*., Phys. Rev. C **68**, 064605 (2003).
[72] H. Seifert *et al*., Phys. Rev. C **47**, 1615 (1993).
[73] A. E. Feldman *et al*., Phys. Rev. C **49**, 2068 (1994).
[74] S. Karataglidis, K. Amos, B. A. Brown, and P. K. Deb, Phys. Rev. C **65**, 044306 (2002).